

STEADY INTERACTION OF A TURBULENT PLANE JET WITH A RECTANGULAR HEATED CAVITY

by

Farida IACHACHENE^a, Amina MATAOUI^{c*}, and Yacine HALOUANE^b

^a Department of Physics, Faculty of Sciences – UMBB, Boumerdes, Algeria

^b Laboratory of Theoretical and Applied Fluid Mechanics, Faculty of Physics, University of Science and Technology Houari Boumediene – USTHB, Algiers, Algeria

^c Laboratory of Energetics, Faculty of Engineering Science – UMBB, Boumerdes, Algeria

Original scientific paper
DOI:10.2298/TSC11311060601

Turbulent heat transfer between a confined jet flowing in a hot rectangular cavity is studied numerically by finite volume method using the $k-\omega$ shear stress tensor one-point closure turbulence model. The location of the jet inside the cavity is chosen so that the flow is in the non-oscillation regime. The flow structure is described for different jet-to-bottom-wall distances. A parametrical study was conducted to identify the influence of the jet exit location and the Reynolds number on the heat transfer coefficient. The parameters of this study are: the jet exit Reynolds number ($1560 < Re < 33333$), the temperature difference between the cavity heated wall and the jet exit ($\Delta T = 60$ °C) and the jet location inside the cavity ($2 \leq L_f \leq 10$ and $2.5 < L_h \leq 10$). The Nusselt number increased and attained its maximum value at the stagnation points and then decreased. The flow structure is found in good agreement with the available experimental data. The maximum local heat transfer between the cavity walls and the flow occurs at the potential core end. The ratio between the stagnation point Nusselt numbers of the cavity bottom, Nu_{B0} , to the maximum Nusselt number on the lateral cavity wall, Nu_{Lmax} , decreased with the Reynolds number for all considered impinging distances. For a given lateral confinement, the stagnation Nusselt number of the asymmetrical interaction $L_h \neq 10$ is almost equal to that of the symmetrical interaction $L_h = 10$.

Key words: jet-cavity interaction, heat transfer, plane jet, turbulence modeling

Introduction

Heat transfers by impinging jets are found in many engineering applications, such as: cooling of turbine blades, tempering of glassware, drying of paper or textile, etc. The knowledge about the local heat transfer coefficient distribution on the incident wall is of great importance for the control processes in any of these applications for high-quality products. A large number of publications on simple geometrical configurations are found in the scientific literature, among them, cases of confined or unconfined circular or rectangular jets impinging on a flat surface. The main variables for jet impingement heat transfer are the jet Reynolds number and the distance of the nozzle relative to the impingement surface. Comprehensive reviews of heat transfer by impinging jets were conducted by Martin [1] and Jambunathan *et al.* [2] for several parameters that also include confinement, submergence, and nozzle geometry; they also considered multiple

* Corresponding author; e-mail: amataoui@usthb.dz; mataoui_amina@yahoo.fr

jets with different array configurations. Martin [1] has also presented studies of the mean fluid flow characteristics of both free and impinging jets. They showed that the Nusselt number increased when the impinging distance is reduced, when Reynolds number increased, or when the mean velocity profile at the exit of the jet nozzle is parabolic. Gardon and Akfirat [3] examined the effect of turbulence level at the nozzle exit on local heat transfer rate for an impinging 2-D jet. They investigated the Nusselt number at the impinging surface as a function of the mean velocity and turbulence intensity. They confirmed the existence of a secondary peak in the radial distribution of the heat transfer coefficient that they attributed to boundary layer transition along the impinging wall. They proposed a correlation for the Nusselt number at the stagnation point as a function of Reynolds number. Another simple geometrical configuration often considered is the case of a two dimensional jet impinging on a curved surface. Kumada *et al.* [4, 5] investigated the local and average heat transfer coefficient on a cylindrical surface interacting with the potential core and the developed regions of a 2-D jet. Gau and Chung [6] examined the heat transfer on a heated semi-cylindrical surface. They considered curvature effects for a concave and convex surface. For convex surfaces, counter rotating vortices near the surface increase the flow momentum and enhance heat transfer near the stagnation point. The increase of surface curvature augments the size of the counter rotating vortices, which increases the Nusselt number at the stagnation point. However, the heat transfer is reduced in the region away from the stagnation point where the flow becomes more stable due to the centrifugal force caused by the effect of the surface curvature. Choi *et al.* [7] studied the fluid flow and heat transfer characteristics of a slot jet impinging on a semi-circular concave surface. They measured the mean and the fluctuating velocity fields and identified the occurrence of a secondary vortex near the curved wall. Numerical study for the same configuration was investigated by Ahmadi *et al.* [8], five different low Reynolds number $k-\epsilon$ models were evaluated to predict the Nusselt number. The results indicate that these models are not suitable to predict reasonably the Nusselt number distribution in the entire impingement surface length. The effects of jet exit Reynolds number and the impinging distance on the local and average circumferential heat transfer distributions from a turbulent air slot jet hitting a semi-circular convex surface was examined experimentally by Chan *et al.* [9]. They proposed a correlation for the stagnation point Nusselt number. A literature review highlighted the insufficiency of research on jet impingement onto a rectangular cavity. Most studies considered heat and mass transfer from the interaction of a slot jet with one or two solid walls, and little research has been devoted to the interactions of jets with a closed bottom cavity [10]. Li and Tao [11] presented both experimental and numerical results of a laminar flow and heat and mass transfer of a slot jet interaction with a rectangular cavity. They found that the average Nusselt number varied as a power-law of Reynolds number. They also found that the effect of the jet exit Reynolds number on the lateral wall was more significant than that of one on the bottom surface. An experimental study on heat transfer behaviors of a confined slot jet impingement was performed by Lin *et al.* [12] for low Reynolds numbers. Two empirical correlations of stagnation and average Nusselt numbers, for $190 \leq Re \leq 1537$ and $1 \leq L_j \leq 8$ were suggested. The $k-\omega$ turbulence model has been used by Benmouhoub and Mataoui [13] to predict the flow resulting from the orthogonal impingement of a plane jet on a moving wall. They found that the heat transfer on the impingement surface is evidenced by the flow with the increasing of the moving surface, many correlations was proposed for the average Nusselt number evolution according to the surface-to-jet velocity ratios for each Reynolds number.

Halouane *et al.* [14] carried out a numerical investigation to predict the fluid flow and heat transfer characteristics of 3-D turbulent a round jet impinging perpendicularly a hot cylindrical cavity using the Reynolds stress model. They show that a reverse flow occurs within

the cavity corner and near the cavity bottom interacted with the main flow producing a toroidal swirl close to the jet exit and they suggested empirical correlation of average Nusselt number according to the impinging distance and Reynolds number.

The jet exit characteristics such as jet mean velocity and turbulent intensity profiles play an important role in heat transfer behaviors. Furthermore, other important parameters, such as the jet Reynolds number and impinging jet distance influencing the heat transfer behaviors of confined impingement slot jets are not yet investigated. The present work reports computations of the fluid flow and thermal fields for plane isothermal fully developed turbulent jet issuing into a rectangular hot cavity, fig.1. The flow produced by a turbulent plane jet into a rectangular cavity can lead to natural self-sustained unsteadiness due to the flapping motion of the jet between the lateral walls of the cavity [15, 16]. This paper considers numerical prediction of heat transfer for the no oscillatory regimes. Two parameters are examined: the location of the jet in the cavity within the zone of occurrence of the no oscillatory regime as described in [15] and the Reynolds number. The phenomenon is steady in average and the predicted data are found to be in good agreement with experimental findings. Two types of steady interaction occur, depending on the jet location in the cavity.

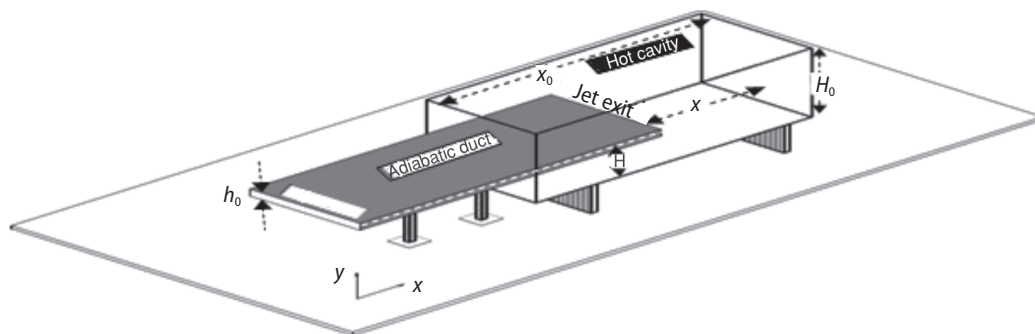


Figure 1. Configuration: jet hot cavity interaction

- The first one called lateral interaction is where the jet flow is deflected to the nearest lateral wall by Coanda effect [17]. From the stagnation lateral point, the flow is divided into two parts; the largest part of the flow is deflected towards the opposite wall while the smaller part is deviated upstream along the nearest wall. In the center of the cavity, far from the cavity walls, a part of the fluid is entrapped in a recirculation zone characterized by a weak velocity.
- The second type called frontal interaction that is a somewhat different interaction, characterized by the deviation of the axis of the jet at the nearest sidewall, impinging the bottom of the cavity. Thus, the jet impinges the cavity bottom obliquely when the jet exit is not located in the mid plane of the cavity. The impingement is perpendicular to the cavity bottom when the jet is located in the symmetrical plane of the cavity.

All interactions (lateral or frontal), the impingement of the jet on the walls produces the splitting of the flow into two parts, which are deflected on each lateral wall. The deflection produces a high-pressure zone near the wall. Calculated pressure contours make clear the occurrence of positive high pressures at the impact zones while low negative pressure zones appear in the region where the two divided jet flows undergo strong curvature effects by 180° deflections. The main pressure is highest at the bottom wall and two smaller secondary maxima occur on each side probably related to the lateral vortices. The splitting of the jet due to impingement produces two lateral eddies at each side of the main jet. The turbulent kinetic energy occurs near

the attachment zone of each lateral deflected flow. In the case of frontal impingement, a zone of maximum energy occurs near the bottom wall at the frontal impact, and a second energetic bubble develops in the region of the two lateral eddies on both sides of the jet. This study extends the previous work in [15] by considering heat transfer effects on no oscillatory regime. The effects of Reynolds number and jet location on local Nusselt number for each cavity wall are examined.

Governing equations

The numerical study was carried out using unsteady Reynolds average Navier-Stokes model (URANS). The fluid is assumed Newtonian and incompressible with constant thermo-physical properties. The URANS equations for incompressible flow in Cartesian co-ordinates are deduced from the mass, momentum, and energy balance equations coupled with the equations of the turbulent quantities:

- mass conservative equation

$$\frac{\partial U_i}{\partial x_i} = 0 \quad (1)$$

- momentum conservation equation

$$\rho \frac{\partial U_i}{\partial t} + \rho U_j \frac{\partial U_i}{\partial x_j} = -\frac{\partial P}{\partial x_i} + \frac{\partial}{\partial x_j} \left(\mu \frac{\partial U_i}{\partial x_j} - \rho \overline{u_i u_j} \right) \quad (2)$$

- energy conservation equation

$$\rho \frac{\partial T}{\partial t} + \rho U_i \frac{\partial T}{\partial x_i} = \frac{\partial}{\partial x_i} \left(\frac{\mu}{Pr} \frac{\partial T}{\partial x_i} - \rho \overline{u_i \theta} \right) \quad (3)$$

where P , T , and U_i are the mean pressure, temperature, and velocity components, respectively, θ and u_i – the fluctuating temperature and velocity components, respectively, x_i is the space co-ordinate, t – the time, and ρ , μ , and Pr are the fluid density, dynamic viscosity, and Prandtl number, respectively.

Turbulence modeling

The URANS modeling is used. The one-point closure turbulent models are based on the concept of Prandtl-Kolmogorov's turbulent viscosity, which is applied in its high Reynolds number form. Thus, the turbulent Reynolds stress tensor and the correlation of the velocity and temperature fluctuations are deduced using algebraic relations (Boussinesq assumption). The closures of the equations are achieved using Shear stress tensor (SST) model energy-specific dissipation rate ($k-\omega$) one-point closure turbulence model. One of the advantages of the $k-\omega$ formulation is the near wall treatment for low Reynolds number computations. The model does not involve the complex non-linear damping functions required for the $k-\varepsilon$ model and is therefore more accurate. A low Reynolds number grid would require a near wall grid resolution for at least $y^+ < 5$. This condition is not verified in most applications, and for this reason, a new near wall treatment was developed for $k-\omega$ model. It allows for a smooth shift from a low Reynolds number form to a wall function formulation. Menter [18] developed the shear stress transport $k-\omega$ model based on two-equation eddy-viscosity turbulence models. The principle of the SST method is to use a $k-\omega$ formulation in the inner parts of the boundary layer and the $k-\varepsilon$ model in the outer part of the boundary layer.

Numerical procedure

The numerical solutions of the governing equations are achieved by the finite volume method. To determine the flow regime, we conducted an unsteady computation for all cases. The time average from the instantaneous values of each physical quantity was done by a post processing treatment. The convection-diffusion terms are discretized using the *power law* schemes for U , V , k , ω , and T and a second order scheme for the pressure. The pressure velocity coupling is resolved by semi-implicit method for pressure linked equation (SIMPLE) algorithm [19]. The solution algorithm is based on internal iterations within each time step. The transport equation in Cartesian co-ordinate of dynamical and thermal characteristics of mean and turbulent flow required for the finite volume method. The boundary conditions for this flow configuration include inflow (inlet), solid wall and outlet as shown in fig. 2. The inlet boundary conditions are:

$$U = U_0, \quad V = 0, \quad k_0 = 0.03U_0^2, \quad \varepsilon_0 = \frac{k_0^{3/2}}{\lambda h_0} (\lambda = 0.1), \quad \omega_0 = \frac{1}{c_\mu} \frac{\varepsilon_0}{k_0}, \quad T = T_0$$

For each wall, the velocity components (U and V) and kinetic energy, k , are set to zero and the specific of dissipation rate ω is set to an asymptotic value proposed by Wilcox [20]. For temperature, the cavity walls are isothermal and kept at constant value, T_w . The duct walls are adiabatic. The dynamic, thermal and geometrical parameters considered in the present study are detailed in fig. 2.

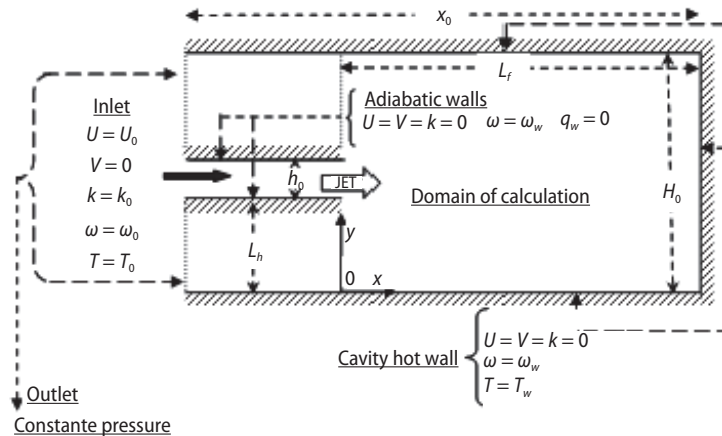


Figure 2. Boundary conditions and parameters

The *outflow* boundary conditions are used. Constant relative static pressure kept at atmospheric level at these boundaries. Structured non-uniform grids are used. Grids refinement before and after the nozzle exit are managed so that the entrainment is described accurately. A sufficiently fine grid is adopted near the cavity and duct walls where a very high gradient of variables prevailed in the viscous sub-layer, fig. 3. For each interaction case a grid independency test is carried out by refining and adjusting the grid in the two directions. It is observed for example for the case ($L_f = 10$ and $L_h = 10$) that fig. 4 shows that grid independence is achieved with 170×130 grid distribution beyond which no further significant change in Nusselt number pro-

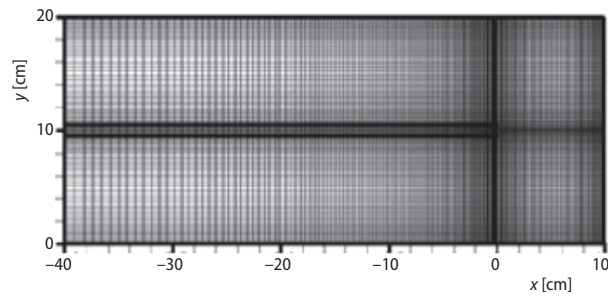
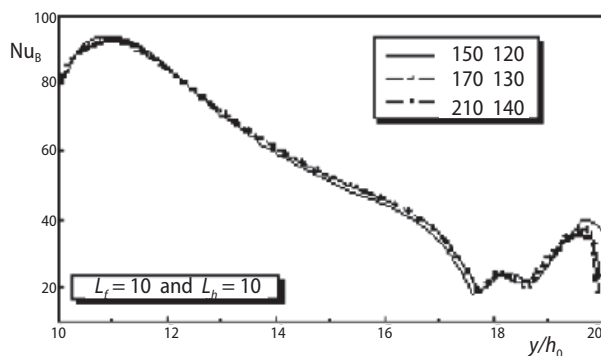
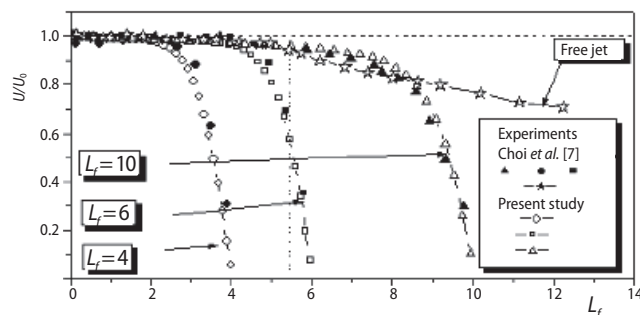
Figure 3. Typical mesh of the jet-cavity ($L_f = 10$)

Figure 4. Effect of grid refinement

Results and discussion

Flow field dynamic

The centerline mean velocity of the jet is calculated for several relative impinging distances L_f (4, 6, and 10) at $Re = 4740$ are shown in fig. 5. Experimental results for a jet impinging on a semi-circular concave surface as well as the results for a free jet. Choi *et al.* [7] also reported in this figure. Comparison shows good agreement for each case. The potential core length can be defined as the length of the region where the axial velocity on the jet centerline stays greater or equal to 95% of the jet exit velocity [2]. The potential core length is about $\approx 5.5 h_0$. The impinging distances considered in fig. 5 are chosen such that for the lowest relative distance ($L_f = 4$), the bottom wall interacted with the potential core region. For the medium distance ($L_f = 6$), the bottom wall is located at the end of the potential core and for the $L_f = 10$, the bottom wall is outside the potential core region. For $L_f = 10$, the potential core is identical to the one found for a free jet. The lateral cavity walls had no significant effect on the potential core length.

Figure 5. Axial velocity evolution along the jet centerline for $Re = 4740$

file is noticed. The grid independence tests are performed for each tested case. The influence of the size of the time step is then tested, which does not affect the case of steady interaction. The residuals of all the variables are less than 10^{-4} for continuity and momentum, and 10^{-6} for energy.

To characterize heat transfer between the jet and the cavity walls, the Nusselt number on each cavity wall, lateral Nusselt number, and bottom Nusselt number are defined:

$$Nu_B(y) = - \left(\frac{h_0}{T_0 - T_w} \right) \left(\frac{\partial T}{\partial x} \right)_{y,wall}$$

and

$$Nu_L(x) = - \left(\frac{h_0}{T_0 - T_w} \right) \left(\frac{\partial T}{\partial y} \right)_{x,wall}$$

Figure 6 shows the distribution of the longitudinal and transversal components of the mean velocity and the turbulent kinetic profiles for $L_f = 40$ and $L_h = 3$ at $Re = 4000$. For validation, these profiles were compared to their corresponding experimental values of Mataoui *et al.* [15]. The experimental and numerical results were found to be in satisfactory agreement. Minor differences were observed in the reverse flow areas and in the near wall regions. They were attributed to the limitation of hot-wire measurements in the recirculating zones. Figure 7(a) evidences the presence of eddies in the cavity when the jet evolves symmetrically inside the cavity, for different axial impinging distances. One notes two stagnation zones corresponding to each cavity wall (bottom and lateral). The jet impinges perpendicularly the cavity bottom and returns towards the exit of the cavity nearest the cavity lateral wall. The reverse flow leaves the cavity with weak velocity entraining the external region of the jet and contributing to the development of two counter rotating eddies on each side of the jet. A low mean velocity, high turbulence energy and a negative pressure due to the Coanda effect [15] characterize these zones. Other circulation regions appear in each cavity corner. The size of the corner eddies increases when the impinging distance decreases as shown in fig. 7(b), which represents an enlargement of one cavity corner.

Heat transfer characteristics

Figure 8 illustrates the local Nusselt number along the cavity bottom for the symmetrical jet ($L_h = 10$) and for different impinging distances ($2.5 < L_f < 10$) at a given $Re = 4700$. The center of the bottom cavity is at $y/h_0 = 10$. For symmetrical interaction, the Nusselt number distributions are symmetrical; only half region is plotted in fig. 8. The Nusselt number at the stagnation region decreased when L_f is increased. For $L_f = 2.5$, it increased by 29% in comparison with the $L_f = 10$ case. The reduction of the local Nusselt number for $L_f = 7.5$ and 10 at the stagnation region is due to the fact that the jet impinges the bottom wall with a weak velocity (outside the potential core). The local Nusselt number exhibited a shifted peak (secondary peak) at around $y/h_0 = 10,55$. The secondary peak corresponded to the interaction of the jet shears layer with the wall. The local Nusselt number increased with increasing y/h_0 distance from the stagnation point to the shifted peak and decreased monotonously while approaching the lateral wall. Close to the lateral wall the Nusselt number increased; this is due to the presence of the vortex in the cavity corner. Many challenges are investigated to explain the physical reasons of the shifted peak. Liu *et al.* [21] and Lytle and Webb [22] suggested that the shifted peak is due to the transition from laminar to turbulent. Goldstein *et al.* [23] attributed it to a vortex ring presence. Merci and Dick [24] related this peak to the off-axis position of the maximum turbulent kinetic energy. This off axis peak is also observed for high Reynolds numbers ($Re > 40000$) and small nozzle-to-plate spacing. Two stagnation zones are observed near the bottom and lateral cavity wall.

The effect of the impinging distance and Reynolds number on the local Nusselt number is examined for each cavity walls (bottom and lateral) and for two impinging distances: $L_f = 2.5$, $L_h = 10$, fig. 9(a) and $L_f = 10$, $L_h = 10$, fig. 9(b). For the cavity bottom wall, the distribution of Nusselt number presents a small inflection which is more evidenced when Reynolds number increases. The maximum near the cavity corner also decrease with Reynolds number. For the case of $L_f = 2.5$ the bottom cavity wall is located in the potential core of the jet. Three peaks are evidenced, the first one correspond to the main stagnation point, the second to the shear layer wall interaction, and the third one is in the vicinity of the cavity lateral wall. The third maximum is due to the eddy within the cavity corner. The size of this eddy is reduced when Reynolds number increases. For the case of $L_f = 10$, the second peak is less evident as L_f increases the same

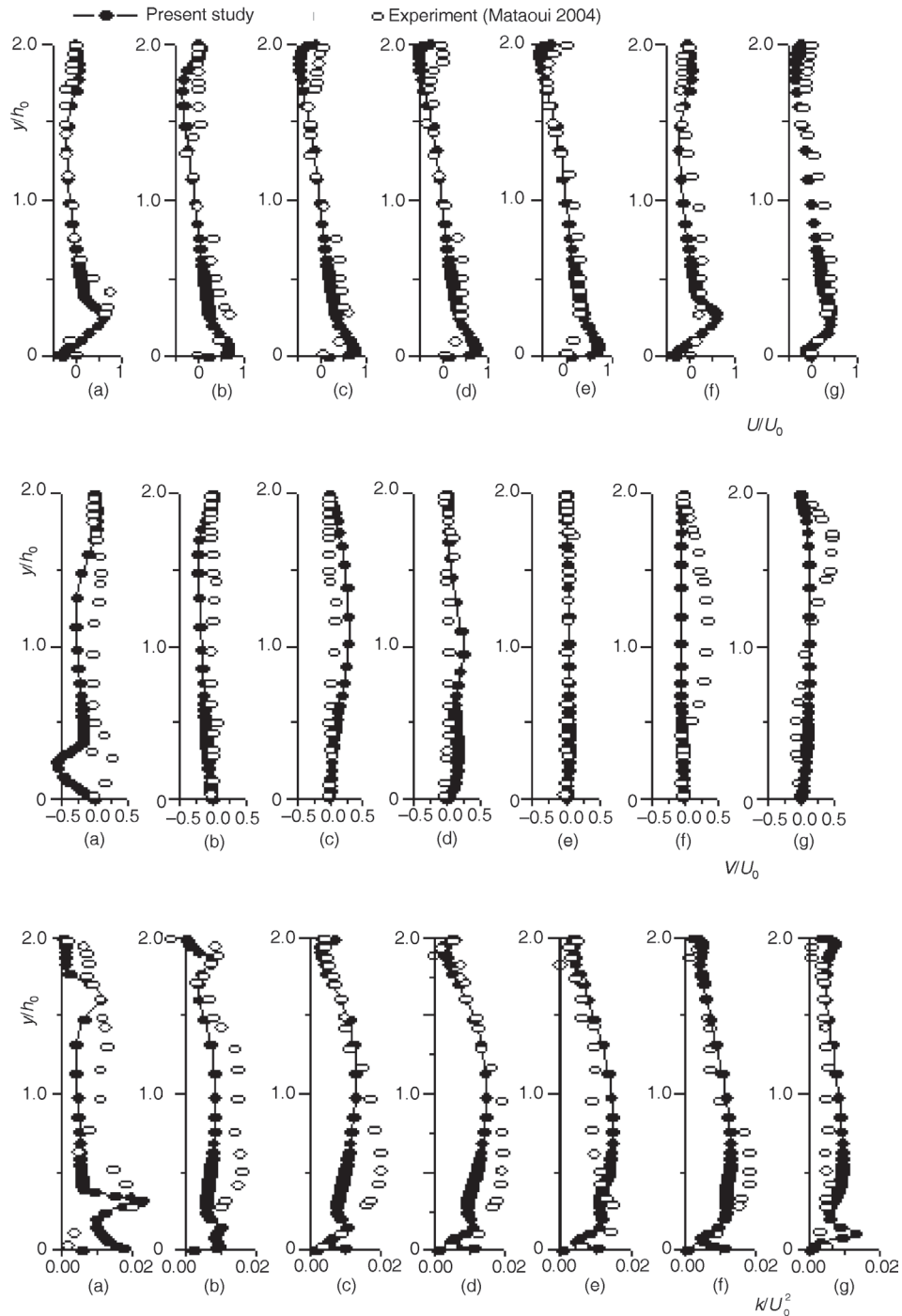


Figure 6. Validation, mean velocity components, and turbulent kinetic energy profiles (closed symbols – present study, open symbols – Mataoui *et al.* (2001) [15]); ($Re = 4000$ and $L_f = 40$ and $L_h = 3$)
 (a) $x/h_0 = 4$, (b) $x/h_0 = 8$, (c) $x/h_0 = 14$, (d) $x/h_0 = 19$, (e) $x/h_0 = 24$, (f) $x/h_0 = 29$, (g) $x/h_0 = 34$

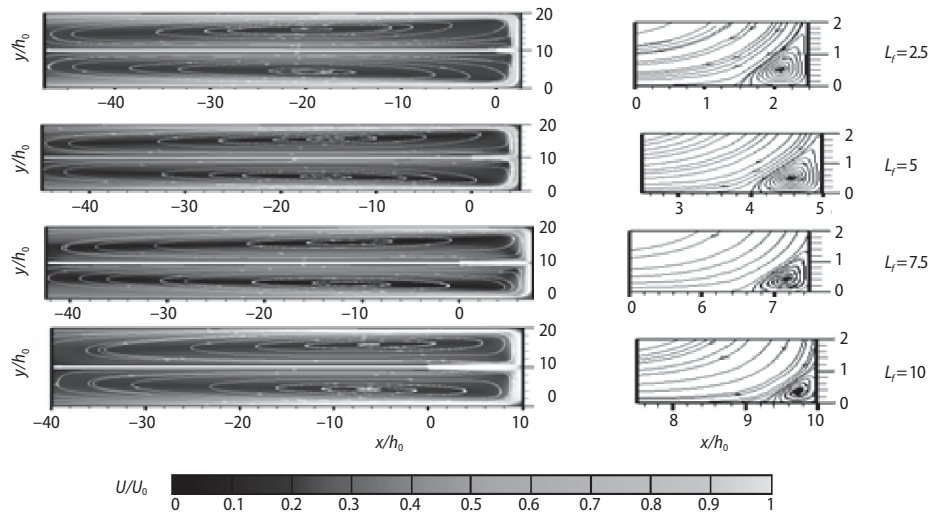


Figure 7. Effect of the impinging distance L_f on dimensionless velocity magnitude (U/U_0) and streamlines contours ($Re = 8000$ and $L_h = 10$)

for the third peak. The eddy of the cavity corner became very small, which disappears when Reynolds increased.

Stagnation heat transfer characteristics

Heat transfer at the stagnation point is represented by Nusselt number in fig. 10. The numerical predictions are compared to the experimental data of Gardon and Akfirat [3]

for a turbulent plane jet impinging perpendicularly a flat plate and of Chan *et al.* [9] for a jet impinging on a semi-circular convex surface. The stagnation Nusselt number evolution is examined for $L_f = 7.5$ and for $Re = 1550-30000$. A good agreement is obtained with these two studies except for small Reynolds numbers. For the symmetrical interaction $L_h = 10$, the ratio between stagnation Nusselt number of the cavity bottom, Nu_{B0} , to the maximum value of the lateral wall Nusselt number, Nu_{Lmax} , decreases with the Reynolds number for all impinging distances as shown in tab. 1.

Average heat transfer characteristics

The average Nusselt number distributions along the cavity bottom wall are calculated and compared with the correlation for a flat surface [1], as shown in fig. 11. It appears that the heat transfer of a confined slot jet impingement is more important than impinging jets without confinement. Figure 12 shows that the average Nusselt numbers increase with jet exit Reynolds number and decrease with an increase of the impinging distance L_f .

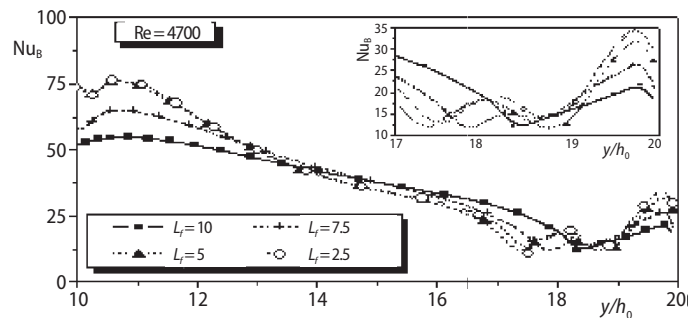


Figure 8. Effect of impinging distance on bottom local Nusselt number ($Re = 4700$ and $L_h = 10$)

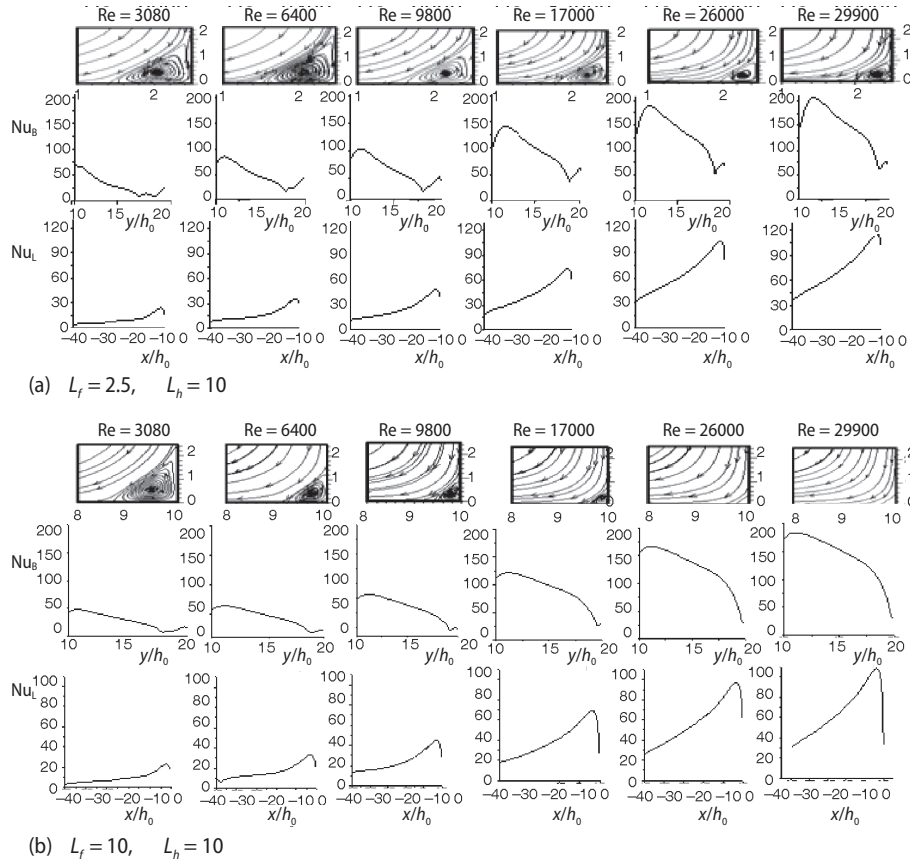


Figure 9. Local Nusselt number along the bottom wall and lateral wall; effect of Reynolds number, (a) $L_f = 2.5, L_h = 10$, (b) $L_f = 10, L_h = 10$

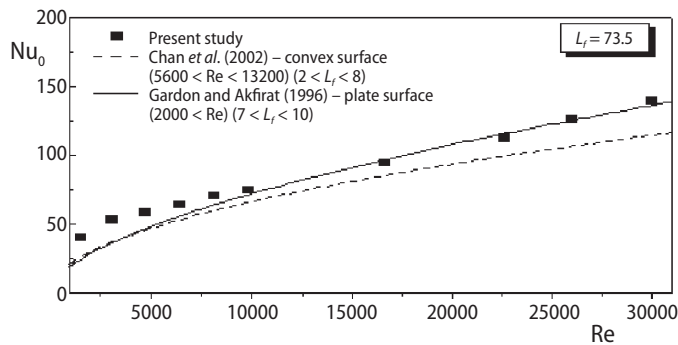


Figure 10. Stagnation bottom Nusselt number vs. Reynolds number ($L_f = 7.5$ and $L_h = 10$)

presented in fig. 14. Similar observations can be made than for the symmetrical interaction ($L_h = 10$): stagnation points correspond to the maximum values of the local Nusselt numbers. The maximum Nusselt number remains equivalent for each lateral confinement: $Nu_{Bmax} \approx \text{constant}$

Asymmetrical interaction

Figure 13 illustrates the isotherms of each symmetrical and asymmetrical interaction. For each ($L_f = 2.5, 5$, and 10 at $Re = 8000$), a similar behavior of the isotherms around the main stagnation point for both type interaction $L_h = 10$ and $L_h = 5$ is observed.

The local Nusselt number for an asymmetrical jet location inside the cavity is

Table 1. Stagnation Nusselt number

Re	Nu_{B0}/Nu_{Lmax}			
	$L_f = 2.5$	$L_f = 5$	$L_f = 7.5$	$L_f = 10$
3080	2.67	2.66	2.22	1.94
6400	2.10	2.14	1.83	1.77
9800	1.80	1.80	1.58	1.63
17000	1.40	1.41	1.32	1.61
33333	1.20	1.31	1.23	1.61

Re	Nu_{Lmax}			
	$L_f = 2.5$	$L_f = 5$	$L_f = 7.5$	$L_f = 10$
3080	23,75	23,62	23,76	23,00
6400	35,60	34,92	34,71	32,94
9800	48,01	47,50	46,97	45,20
17000	73,62	72,57	71,46	69,08
33333	126,71	125,06	123,20	118,94

Re	Nu_{B0}			
	$L_f = 2.5$	$L_f = 5$	$L_f = 7.5$	$L_f = 10$
3080	63,22	62,94	52,72	44,60
6400	74,80	74,62	63,63	58,41
9800	86,27	85,56	74,07	73,68
17000	102,98	102,86	94,10	111,06
33333	152,46	162,95	151,02	190,12

for a given Reynolds number and a given jet height L_h . The impinging distance L_f influences the lateral maximum Nusselt number: Nu_{Bmax} varies for a given Reynolds number and a given jet height L_h .

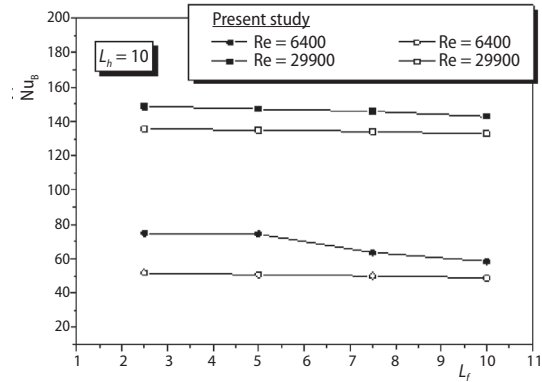


Figure 11. Average bottom Nusselt numbers

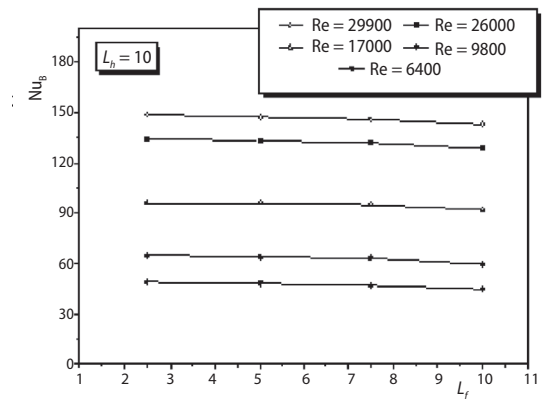


Figure 12. Effect of Reynolds number

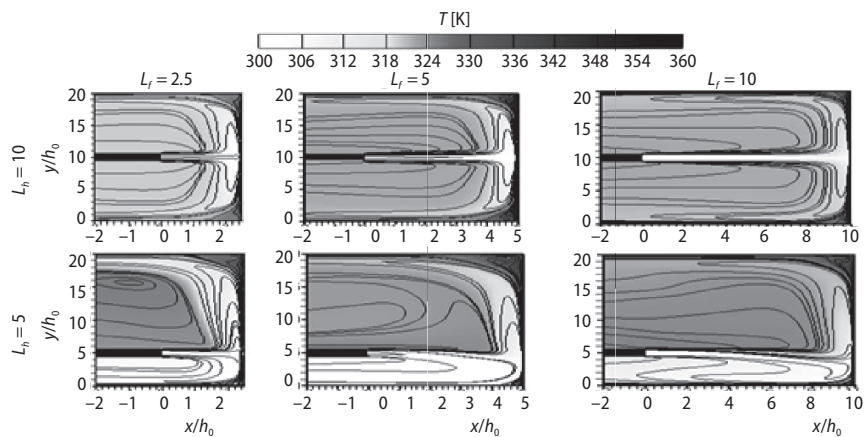


Figure 13. Isotherms [K] symmetrical interaction $L_h = 10$ and asymmetrical interaction $L_h = 5$ ($L_f = 2.5; 5, \text{ and } 10$ Re = 8000)

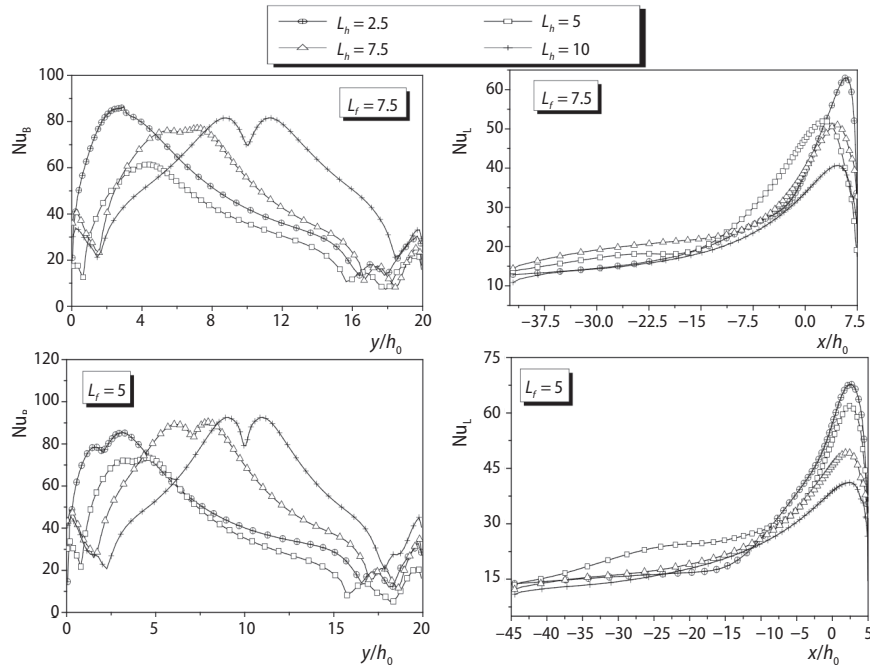


Figure 14. Effect of the height of the jet inside the cavity (L_h) $Re = 8000$

Conclusions

Numerical investigation of heat transfers between a slot jet issuing into a rectangular hot cavity is conducted. The effect of confinement on heat transfer is evaluated for varying parameters such as the jet location in the cavity ($2 < L_f < 10$ and $2.5 < L_h < 10$) and Reynolds number ($1560 < Re < 33333$). The present study shows that the heat transfer characteristics of the confined impinging slot jet are not similar to those of the unconfined impinging slot jet. The effect of lateral cavity walls on flow and thermal field is significant. The decay rate of heat transfer for confined slot jet impingement is much more important than that of impinging jets without confinement. The flow structures agree well with available experimental data. The maximum local heat transfer between the cavity walls and the flow is observed at the potential core end. The ratio between the stagnation point Nusselt numbers of the cavity bottom to the maximum Nusselt number on the lateral cavity wall diminishes when Reynolds number decreases for all considered jet locations. For each lateral confinement, the stagnation Nusselt number of the asymmetrical interaction or symmetrical interaction is almost constant. However, the heat transfer experimental investigation is highly recommended for the confirmation of the numerical predictions and will be performed in the future.

Nomenclature

H	– height of the jet exit, [m]	L_h	– non-dimensional jet height, ($= H/h_0$), [–]
h_0	– nozzle thickness, [m]	Nu_B	– local Nusselt number on the bottom wall, [–]
k	– turbulent kinetic energy, [m^2s^{-2}]	Nu_L	– local Nusselt number on the lateral wall, [–]
L_f	– non-dimensional impinging distance, ($= X/h_0$), [–]		

Nu_{B0}	– stagnation point Nusselt number on the bottom wall, [-]	U	– axial mean velocity, [ms^{-1}]
Nu_{Lmax}	– maximum Reynolds number on the lateral wall, [-]	U_0	– jet exit mean velocity, [ms^{-1}]
\overline{Nu}_B	– average Nusselt number on the bottom wall, [-]	V	– radial mean velocity, [ms^{-1}]
P	– mean pressure, [Pa]	X	– location of the jet exit, [m]
Pr	– Prandtl number, [-]	<i>Greek symbols</i>	
Re	– Reynolds number, ($= U_0 h_0 / \nu$), [-]	ε	– dissipation of turbulent energy, [$m^2 s^{-3}$]
T	– mean temperature, [K]	μ	– turbulent eddy viscosity, [$kg \cdot m^{-1} s^{-1}$]
T_w	– wall temperature, [K]	ν	– kinematic viscosity, [$m^2 s^{-1}$]
		ρ	– fluid density, [$kg m^{-3}$]
		ω	– specific dissipation rate, [s^{-1}]

References

- [1] Martin, H., Heat and Mass Transfer between Impinging Gas Jets and Solid Surfaces, *Advances in Heat Transfer*, 13 (1977), pp. 1-60
- [2] Jambunathan, K., et al., A Review of Heat Transfer Data for Single Circular Jet Impingement, *International Journal of Heat and Fluid Flow*, 13 (1992), 2, pp. 106-115
- [3] Gardon, R., Akfirat, J. C., Heat Transfer Characteristics of Impinging Two Dimensional Air Jets, *Journal Heat Transfer*, 88 (1966), 1, pp 101-107
- [4] Kumada, M., et al., Mass Transfer on a Cylinder in the Potential Core Region of a Two-Dimensional Jet, *Heat Transfer – Japanese Research*, 2 (1973), 3, pp. 53-66
- [5] Kumada, M., et al., Mass Transfer on a Cylinder in Developed Region of a Two Dimensional Jet, *Heat Transfer – Japanese Research*, 5 (1976), Sep., pp. 1-13
- [6] Gau, C., Chung, C. M., Surface Curvature Effect on Slot-Air Jet Impingement Cooling Flow and Heat Transfer Process, *Journal of Heat Transfer*, 113 (1991), 4, pp. 858-864
- [7] Choi, M., et al., Measurements of Impinging Jet Flow and Heat Transfer on a Semi-Circular Concave Surface, *International Journal of Heat and Mass Transfer*, 43 (2000), 10, pp. 1811-1822
- [8] Ahmadi, H., et al., Numerical Modeling of a Turbulent Semi-Confined Slot Jet Impinging on a Concave Surface, *Thermal Science*, 19 (2015), 1, pp. 129-140
- [9] Chan, T. L., et al., Heat Transfer Characteristics of a Slot Jet Impinging on a Semi-Circular Convex Surface, *International Journal of Heat and Mass Transfer*, 45 (2002), 5, pp. 993-1006
- [10] Zuckerman, N., Lior, N., Jet Impingement Heat Transfer: Physics, Correlations, and Numerical Modeling, *Advances in Heat Transfer*, 39 (2006), pp. 565-631
- [11] Li, P. W., Tao, W. Q., Numerical and Experimental Investigations on Heat/Mass Transfer of Slot-Jet Impingement in a Rectangular Cavity, *International Journal Heat and Fluid Flow*, 14 (1993), 3, pp. 246-253
- [12] Lin, Z. H., et al., Heat Transfer Behaviors of a Confined Slot Jet Impingement, *International Journal Heat and Mass Transfer*, 40 (1997), 5, pp. 1095-1107
- [13] Benmouhoub, D, Mataoui, A., Computation of Heat Transfer of a Plane Turbulent Jet Impinging a Moving Plate, *Thermal Science*, 18 (2014), 4, pp. 1259-1271
- [14] Halouane, Y., et al., Turbulent Heat Transfer for Impinging Jet Flowing Inside a Cylindrical Hot Cavity, *Thermal Science*, 19 (2015), 1, pp. 141-154
- [15] Mataoui, A., et al., Flow Regimes of Interaction of a Turbulent Plane Jet into a Rectangular Cavity: Experimental Approach and Numerical Modeling, *Journal of Flow, Turbulence, and Combustion*, 67 (2001), 4, pp. 267-304
- [16] Mataoui, A., Schiestel, R., Unsteady Phenomena of an Oscillating Turbulent Jet Flow Inside a Cavity: Effect of Aspect Ratio, *Journal of Fluids and Structures*, 25 (2009), 1, pp. 60-79
- [17] Bourque, C., Newman, B. G., Reattachment of a Two-Dimensional, Incompressible Jet to an Adjacent Flat Plate, *Aeronautical Quarterly*, 11, (1960), 3, pp. 201-232
- [18] Menter, F. R., Two-Equation Eddy-Viscosity Turbulence Models for Engineering Applications, *AIAA Journal*, 32 (1994), 8, pp. 1598-1605
- [19] Patankar, S. V., Numerical Heat Transfer and Fluid Flow, in: *Series in Computational Methods in Mechanics and Thermal Sciences*, 1st ed., Hemisphere Publ., Corp., N. Y., USA, 1980
- [20] Wilcox, D. C., *Turbulence Modeling for CFD*, 2nded., DCW Industries, Inc., La Canada, Cal., USA, 1998
- [21] Liu, Q., et al., Application of Pressure and Temperature Sensitive Paints for Study of Heat Transfer to a Circular Impinging Air Jet, *International Journal of Thermal Sciences*, 47 (2008), 6, pp 749-757

- [22] Lytle, D., Webb, B. W, Air Jet Impingement Heat Transfer at Low Nozzle-Plate Spacing, *International Journal of Heat and Mass Transfer*, 37 (1994), 12, pp. 1687-1697
- [23] Goldstein, R. J., *et al.*, Stream Wise Distribution of the Recovery Factor and the Local Heat Transfer Coefficient to an Impinging Circular Air Jet, *International Journal of Heat and Mass Transfer*, 29 (1986), 8, pp. 1227-1235
- [24] Merci, B., Dick, E., Heat Transfer Predictions with a Cubic $k-\varepsilon$ Model for Axisymmetric Turbulent Jets Impinging onto a Flat Plate, *International Journal of Heat and Mass Transfer*, 46 (2003), 3, pp. 469-480